Atom physics and physics of clusters and nanostructures

Original article
UDC 536.423
DOI: https://doi.org/10.18721/JPM.19108

SIZE-DEPENDENT ADSORPTION AND ELECTRONIC MODULATION OF PYRENE NANOSTRUCTURES TOWARD TOXIC GAS DETECTION: A DFT STUDY

R. H. Khalaf ✉, M. L. Jabbar

University of Thi-Qar, An Nasiriyah, Republic of Iraq

✉ rihab.khalaf@utq.edu.iq

Abstract. The DFT-study at the B3LYP/6-31G level has been conducted to analyze the interactions of pyrene-based graphene fragments with toxic gases F_2, AsH_3, PH_3, and HF. Three diamond-shaped *n*-pyrene clusters (n = 3, $C_{30}H_{14}$; n = 4, $C_{48}H_{18}$; n = 5, $C_{70}H_{22}$) were systematically optimized, and their adsorption behavior was investigated through the total and adsorption energies, frontier molecular orbital (HOMO − LUMO) distributions, and energy gaps. The results revealed that gas adsorption induces significant modifications in the electronic structure of the pyrene clusters, with variations depending on both the cluster size and gas nature. The calculated adsorption energies demonstrated a size-dependent trend, indicating that increasing the number of zigzag edges in pyrene enhances surface reactivity toward certain analytes. These findings highlight the potential of pyrene-based graphene nanostructures as selective and efficient sensors for hazardous gases.

Keywords: graphene, pyrene, toxic gas, adsorption, DFT, cluster size, molecular orbital, energy gap, gas detection

For citation: Khalaf R. H., Jabbar M. L., Size-dependent adsorption and electronic modulation of pyrene nanostructures toward toxic gas detection: a DFT study, St. Petersburg State Polytechnical University Journal. Physics and Mathematics. 19 (1) (2026) 91–105. DOI: https://doi.org/10.18721/JPM.19108

Научная статья
УДК 536.423
DOI: https://doi.org/10.18721/JPM.19108

АДСОРБЦИЯ И ЭЛЕКТРОННАЯ МОДУЛЯЦИЯ НАНОСТРУКТУР ПИРЕНА, ДЕТЕКТИРУЮЩИХ ТОКСИЧНЫЕ ГАЗЫ: ИССЛЕДОВАНИЕ ЗАВИСИМОСТЕЙ ЭТИХ ХАРАКТЕРИСТИК ОТ РАЗМЕРА КЛАСТЕРОВ ПИРЕНА МЕТОДОМ ФУНКЦИОНАЛА ПЛОТНОСТИ

Р. Х. Халаф ✉, М. Л. Джаббар

Университет Ди-Кар, г. Эн-Насирия, Республика Ирак

✉ rihab.khalaf@utq.edu.iq

Аннотация. В проведенном теоретическом исследовании использована теория функционала плотности (DFT) на уровне B3LYP/6-31G для изучения взаимодействия наноструктур на основе графена (с базой из пирена) с такими токсичными газами, как газообразный фтор, арсин, фосфин и фтороводород (F_2, AsH_3, PH_3 и HF, соответственно). Нами систематически оптимизированы три ромбовидных кластера пирена с

разными значениями их размера n и проанализированы их адсорбционные и электронные свойства: общая энергия, энергия адсорбции, распределение молекулярных орбиталей и энергетические зазоры HOMO − LUMO. Установлено, что в результате адсорбции газа кластеры пирена претерпевают значительные изменения электронной структуры, зависящие как от размера кластера, так и от природы газа. Рассчитанные значения энергии адсорбции зависят от размера n, что указывает на повышение реакционной способности поверхности к анализируемым токсичным газам при увеличении количества зигзагообразных краев в пирене. Полученные результаты подтверждают высокий потенциал графеновых наноструктур на основе пирена в качестве селективных и эффективных чувствительных элементов опасных газов для создания устройств.

Ключевые слова: графен, пирен, ядовитый газ, адсорбция, метод функционала плотности, размер кластера, молекулярная орбиталь, энергетичекий зазор

Для цитирования: Халаф Р. Х., Джаббар М. Л. Адсорбция и электронная модуляция наноструктур пирена, детектирующих токсичные газы: исследование зависимостей этих характеристик от размера кластеров пирена методом функционала плотности // Научно-технические ведомости СПбГПУ. Физико-математические науки. 2026. Т. 19. № 1. С. 91–105. DOI: https://doi.org/10.18721/ JPM.19108

Introduction

Graphene nanoflakes (GNFs) exhibit diverse structural properties influenced by their shape, size [1], and edge terminations. Among these, the diamond-shaped graphene (i.e. rhomboid-shaped or pyrene) structures are of particular interest making them promising candidates for applications in nanoelectronics [2], spintronics, and quantum computing. Despite extensive interest, research on diamond-shaped GNRs formed by fusing triangular graphene units remains limited. Recent advances have highlighted the need to further explore the electronic and magnetic characteristics of such novel GNR architectures, but they remain insufficiently explored [3 − 5]. Recent studies have focused on diamond-shaped GNFs formed from fused benzenoid rings, exploring their tunable electronic behavior [6]. Notably, configurations like zigzag-edged and triangular GNFs show potential for magnetism and unique electronic responses.

Graphene, with its well-defined sp^2-hybridized carbon lattice [7, 8], a two-dimensional material with a hexagonal lattice structure [9], carbon-based nanomaterials [10], including graphene [11], carbon nanotubes, and fullerenes, have gained significant attention for their outstanding physicochemical properties and wide applicability in energy storage, gas adsorption, and electronic devices [12, 13]. Graphene displays edge-dependent phenomena influenced by geometry and confinement effects. These nanoribbons, typically with zigzag or armchair edges, show tunable electronic, magnetic, and optical properties, making them attractive for nanoscale [14] device applications [15]. However, its lack of an intrinsic bandgap limits its use in transistor-based devices. A practical solution is to divide graphene into nanoscale fragments, known as graphene nanoflakes (GNFs), whose properties are highly dependent on their geometry and edge configuration [16]. Among graphene-derived structures [17], graphene nanoribbons (GNRs) offer tunable electronic behavior due to their reduced dimensionality and edge effects [18], with zigzag-edged GNRs showing strong potential for enabling spintronic and electronic device functionality [19], where graphene-related materials (GRMs) offer high sensitivity and selectivity for detecting hazardous gases [20 − 22]. Due to their unique structure and reactivity, GRMs are considered as promising candidates for next-generation gas sensors in environmental and workplace safety monitoring [23].

The aim of this study is to design n-pyrene as sensors for highly toxic gases (such as F_2, AsH_3, PH_3, and HF) that are harmful to living organisms in general (and humans in particular) by studying the electronic properties; for instance, energy gap, ionization potential, electron affinity, hardness, and softness, as well as adsorption energy, and then predicting the possibility of applying them in sensor devices.

Computational details

All quantum calculations were carried out within Kohn – Sham density-functional theory using the hybrid B3LYP functional [24]. The model system was a diamond-shaped graphene nanoflake (pyrene) constructed from sp^2 carbon atoms; all edge carbons were hydrogen-terminated to remove dangling bonds. Unless noted otherwise, calculations were performed with the 6-31G valence-split basis on all atoms (H, C). For better numerical stability, geometries were fully optimized without symmetry constraints using Geo-Opt until the force reached the lowest minimum energy. Harmonic frequency analyses at the same level confirmed that all stationary points were true minima (no imaginary frequencies) and provided zero-point energies and thermochemical corrections at 298 K and 1 atm.

Electronic properties were evaluated on the optimized structures. Frontier orbital energies (HOMO/LUMO) and the energy gap were taken directly from the orbital eigenvalues. Density of states (DOS) was obtained by Gauss Sum according to the eigenvalue of the spectrum. Charge analysis was performed through Mulliken and Hirshfeld schemes, and global electronic properties and dipole moments were extracted from the analytic derivatives. For physisorption studies on the GNF surface, adsorbates were placed at several initial sites.

Results and discussion

Molecular structure. The *n*-pyrene structures were modeled by systematically varying the number of zigzag edges, with $n = 3$, 4, and 5, corresponding to chemical formulas $C_{30}H_{14}$, $C_{48}H_{18}$, and $C_{70}H_{22}$, respectively. These variations enabled a controlled study of edge effects on the adsorption properties. To probe the interaction of graphene with hazardous pollutants, four toxic gas molecules: fluorine (F_2), arsine (AsH_3), phosphine (PH_3), and hydrogen fluoride (HF) were selected as adsorbates due to their industrial relevance and high toxicity.

Each gas molecule was initially placed near the most chemically active regions of the graphene surface, allowing for multiple adsorption configurations to be considered. All systems underwent full geometric optimization using density functional theory (DFT) within the B3LYP functional and 6-31G basis set, ensuring the identification of stable configurations without imaginary frequencies. Subsequent analyses included adsorption energy calculations, frontier molecular orbital (FMO) analysis, and evaluation of dipole moment changes to elucidate the impact of gas adsorption on the electronic structure of diamond-shaped graphene.

The optimized configurations in Fig. 1, *a*, *b*, and c illustrate the interaction between diamond-shaped graphene nanoflakes ($n = 3$, 4, and 5 respectively) and four toxic gas molecules: gaseous fluorine (F_2), arsine (AsH_3), phosphine (PH_3) and hydrogen fluoride (HF). The calculated equilibrium distances indicate the strength and nature of adsorption.

For $n = 3$, F_2 gas exhibits the shortest adsorption distance (2.29 Å), suggesting strong physisorption with potential partial charge transfer to the graphene π-system. HF gas shows a moderately strong interaction at 4.67 Å, consistent with hydrogen bonding or weak electrostatic attraction. AsH_3 and PH_3 gases display larger separations (3.76 Å and 3.92 Å), implying weaker

a)

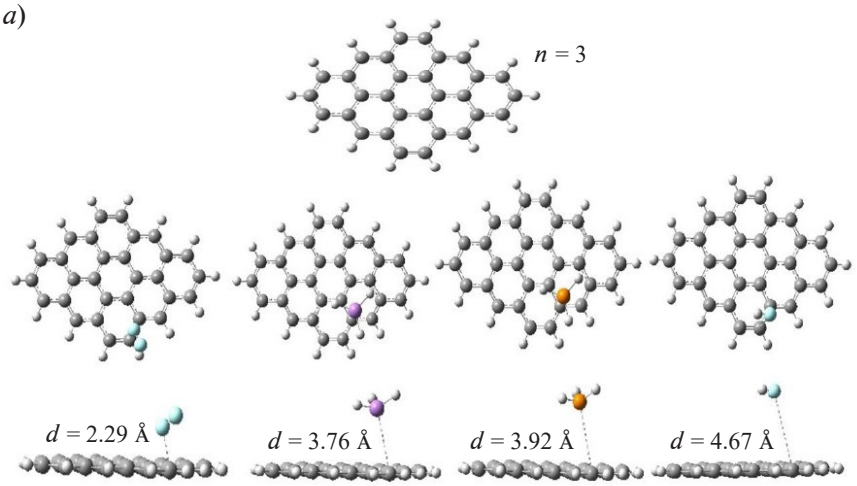

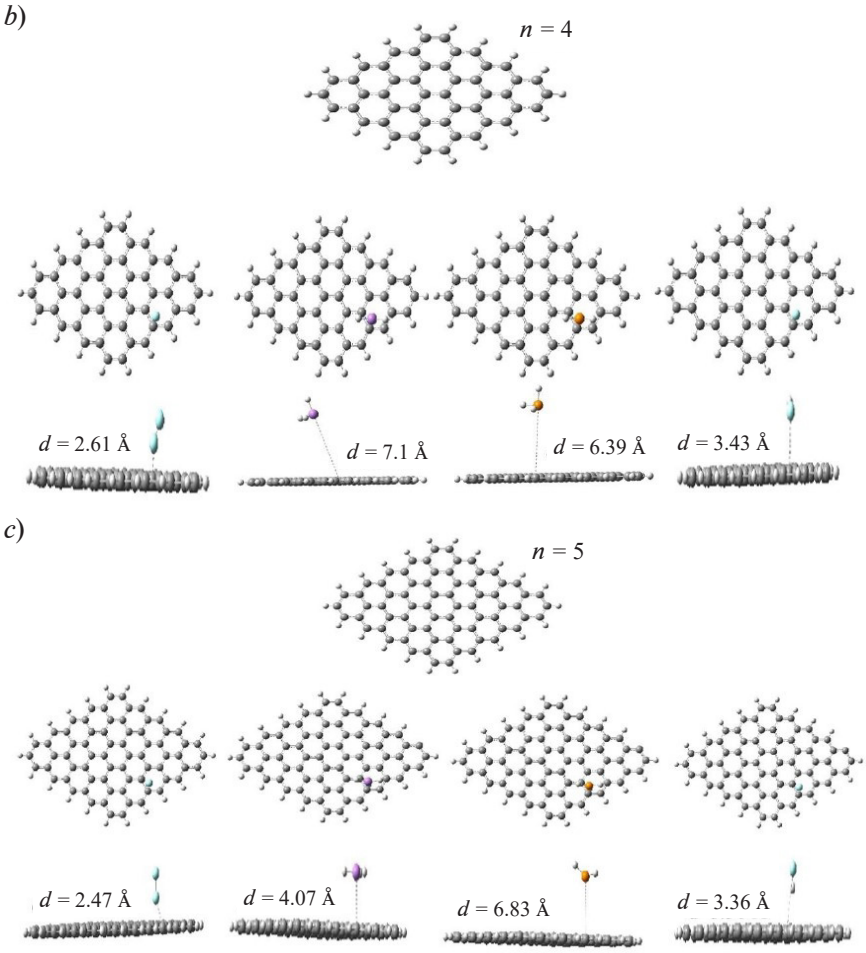

Fig. 1. Structure types of pristine *n*-pyrene molecules with different *n* values. The molecules have adsorbed high toxic gases (F_2, AsH_3, PH_3, and HF). $n = 3$ (*a*), 4 (*b*), 5 (*c*); *d* is the calculated equilibrium adsorption distance

Van der Waals forces dominating the adsorption mechanism. For $n = 4$, notable variations in interaction distances are observed, particularly with AsH_3 (7.10 Å) and PH_3 (6.39 Å), which indicate minimal adsorption and a likely repulsive interaction regime. In contrast, HF adsorption shortens to 3.43 Å, while F_2 slightly increases to 2.61 Å, reflecting size and edge effects on surface reactivity.

The increased flake size ($n = 4$) introduces a more extended π-system, which can delocalize charge density over a broader area, thereby reducing localized binding strengths for certain gases. For $n = 5$, the adsorption distance also illustrates the shorter length than that for $n = 4$ except for the structure interaction with PH_3 gas. These indicate the greatest adsorption and a likely attractive interaction regime. Overall, the results highlight that adsorption strength is highly sensitive to all the edge configurations (*n* value) and the chemical nature of the adsorbate, with F_2 and HF showing the highest affinities across each structure, while AsH_3 and PH_3 exhibit weak physisorption, particularly for large flakes. These findings suggest that tuning the graphene flake size can selectively enhance sensing capabilities toward specific toxic gases.

Density of states. The density of states (DOS), which offers a straightforward method of characterizing intricate electronic structures, is arguably the most crucial idea for comprehending the physical characteristics of materials. The band gap is one of the important parameters that the DOS makes visual and characterizes the electrical and optical properties of materials. The capacity to analyze and adjust different material properties is significantly enhanced by the computation of a high-quality DOS that accurately represents a material's electronic structure. The availability and simplicity of Density Functional Theory (DFT) calculations have made DOS calculations commonplace today [25 – 27].

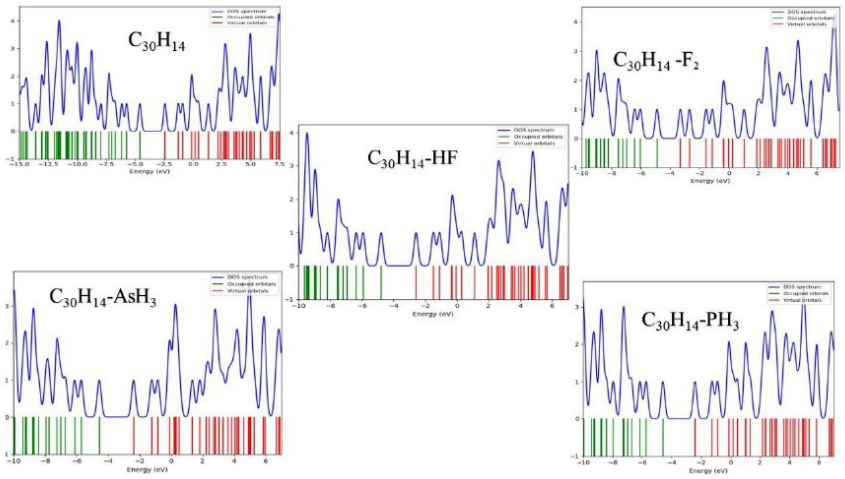

Fig. 2. DOS for pristine 3-pyrene ($C_{30}H_{14}$) adsorbed high toxic gases (F_2, AsH_3, PH_3 and HF)

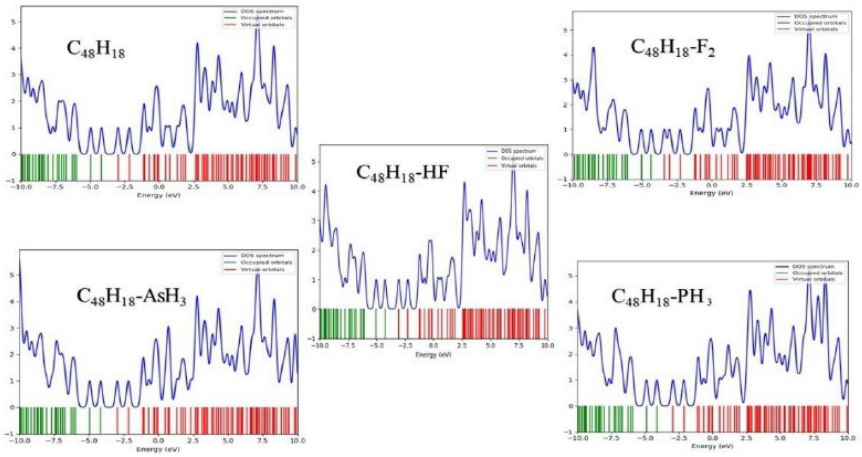

Fig. 3. DOS for pristine 4-pyrene ($C_{48}H_{18}$) adsorbed the same high toxic gases

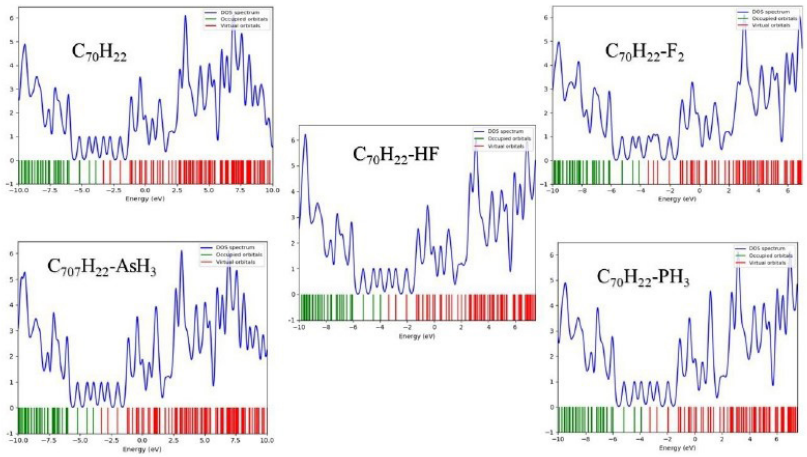

Fig. 4. DOS for pristine 5-pyrene ($C_{70}H_{22}$) adsorbed the same high toxic gases (F_2, AsH_3, PH_3 and HF)

Table 1

Extracted DOS parameters for pyrene nanostructures under toxic gas adsorption

Structure	Parameter value, eV		DOS Intensity, a.u.
	E_{peak}(VB)	E_{peak}(CB)	
3-pyrene (3P)			
Pristine 3P	–1.20	1.10	–
3P–F_2	–0.90	0.68	0.45
3P–AsH_3	–1.15	1.04	0.22
3P–PH_3	–1.14	1.05	0.20
3P–HF	–1.05	1.09	0.33
4-pyrene (4P)			
Pristine 4P	–0.63	0.59	–
4P–F_2	–0.49	0.44	0.41
4P–AsH_3	–0.61	0.60	0.15
4P–PH_3	–0.59		0.14
4P–HF	–0.57	0.64	0.29
5-pyrene (5P)			
Pristine 5P	–0.34	0.29	–
5P–F_2	–0.33	0.30	0.25
5P–AsH_3			0.17
5P–PH_3			0.15
5P–HF			0.22

Notations: E_{peak} (VB), E_{peak} (CB) are peak positions of valence and conduction bands, relatively.

Footnotes: the Fermi energy is set $E_F = 0$ eV in all cases; the DOS intensity is given relative to pristine pyrene.

The density of states (DOS) profiles for pristine pyrene nanoflakes ($C_{30}H_{14}$, $C_{48}H_{18}$, and $C_{70}H_{22}$) and their complexes with high-toxic gases (F_2, AsH_3, PH_3, and HF) reveal significant alterations in electronic structure upon adsorption (see Figs. 2 – 4). For pristine pyrene (diamond-shaped (GNF)), the DOS spectrum exhibits a well-defined $\pi - \pi^*$ separation, corresponding to the intrinsic band gap.

The introduction of toxic gas molecules induces notable modifications in the DOS near the Fermi level, indicating charge transfer and hybridization effects between the adsorbates and surface of the graphene framework (see Table 1). In structure $C_{30}H_{14}$, the adsorption of F_2 and HF results in a pronounced increase in DOS intensity near the conduction band edge, signifying enhanced electron-accepting characteristics, consistent with the high electronegativity of fluorine. Conversely, AsH_3 and PH_3 introduce localized states within the band gap, likely due to weaker orbital overlap, suggesting physisorption with partial charge redistribution. While, for the larger nanoflakes ($C_{48}H_{18}$ and $C_{70}H_{22}$), the DOS spectra demonstrate more delocalized π-electron interactions and reduced bandgaps upon gas adsorption, highlighting stronger electronic coupling.

In particular, the gas of HF adsorption shows substantial DOS broadening near the Fermi level, which could enhance electrical conductivity and sensor sensitivity. The variation in DOS responses with flake size suggests that quantum confinement effects diminish with increasing system size, allowing greater charge delocalization. As a result of the DOS modifications carried out, the potential of the diamond-shaped graphene nanoflakes is confirmed as selective and

size-tunable sensing platforms for detecting toxic gases, where the nature of interaction chemisorption versus physisorption can be inferred from the degree of DOS perturbation and gap narrowing.

Frontier energy. The energy gap represents the conductive and insulating properties of material, defined as the energy difference between the highest occupied molecular orbital (HOMO) and the lowest unoccupied molecular orbital (LUMO) [28 – 30].

Table 2

The values of HOMO, LUMO energies, an energy gap of pristine pyrene (n = 3 – 5), and that with toxic gases

System	Energy, eV		
	E_{HOMO}	E_{LUMO}	E_{gap}
3-pyrene (3P)			
Pristine 3P	–4.596	–2.313	2.283
3P–F_2	–4.890	–3.312	1.578
3P–AsH_3	–4.569	–2.381	2.187
3P–PH_3	–4.593	–2.406	
3P–HF	–4.778	–2.588	2.190
4-pyrene (4P)			
Pristine 4P	–4.171	–2.952	1.219
4P–F_2	–4.347	–3.413	0.934
4P–AsH_3	–4.169	–2.951	1.218
4P–PH_3	–4.134	–2.937	1.197
4P–HF	–4.256	–3.055	1.200
5-pyrene (5P)			
Pristine 5P	–3.919	–3.289	0.630
5P–F_2	–4.107	–3.479	0.628
5P–AsH_3	–3.925	–3.295	0.630
5P–PH_3	–3.904	–3.274	
5P–HF	–3.977	–3.345	0.633

The results listed in Table 2 show that the E_{HOMO} and E_{LUMO} values represent the energy of the highest fully occupied orbital and the energy of the lowest empty orbital respectively, which are related to the ionization potential, and electron affinity respectively. Subsequently, this relationship between E_{HOMO}, E_{LUMO}, and E_{gap} provides a direct understanding of the effect of adsorption on electronic properties and the potential for designing sensitive materials tailored to specific gas species. An analysis of the data in Table 1 and Fig. 5, allows us to note that the energy gap of 3-pyrene structure (2.283 eV) decreases significantly upon adsorption of F_2 (1.578 eV), indicating a strong interaction and charge transfer from pyrene to the adsorbed molecule due to the high electronegativity of fluorine, which increases conductivity. Meanwhile, AsH_3, PH_3, and HF gases exhibit similar energy gaps (from ~2.187 to 2.190 eV), suggesting relatively weaker interactions and closer to a physical nature (physisorption). For 4-pyrene (n = 4), the energy gap of the pure surface is smaller (1.219 eV), reflecting increased conductivity due to the increased volume and reduced quantum confinement effect. Adsorption with F_2 reduces the gap to 0.934 eV, indicating a strong chemical interaction that increases the electron density near the Fermi level. Such gases as AsH_3, PH_3, and HF maintain the band gap in the range from ~1.197 to 1.218 eV, indicating limited electronic influence compared to that of F_2. In 5-pyrene, the surface exhibits a very small band gap (0.630 eV), which is suitable for highly sensitive sensing applications. Adsorption with all gases results in very small changes in the band gap (~0.628 – 0.633 eV), indicating that the large size reduces the sensitivity of the band gap to changes due to adsorption, although changes in the E_{HOMO} and E_{LUMO} positions can be observed, reflecting charge redistribution at the surface.

The results of data analysis. The achieved results are in good agreement with previous density functional theory investigations on graphene-based nanostructures used for gas sensing [3, 31], revealed that adsorption of small toxic molecules on diamond-shaped graphene nanoflakes leads to a noticeable reduction in the HOMO – LUMO energy gap, typically within 0.5 – 1.0 eV, consistent with our finding that F_2 adsorption decreases the gap from 2.28 to 1.57 eV for the n = 3 pyrene system. Similarly, the calculated adsorption energies for AsH_3 (–2.09 eV) and PH_3 (–1.30 eV) fall within the range reported in earlier studies on gas – graphene interactions, confirming the strong donor-acceptor character of these systems.

Furthermore, the observed increase in electron affinity and softness after adsorption agrees with trends reported for other sp^2 carbon materials, where enhanced charge transfer improves sensing sensitivity. These consistencies with literature data validate the reliability of the present

computational approach (B3LYP/6-31G) and emphasize that the size-dependent modulation of electronic properties plays a dominant role in determining the adsorption behavior of pyrene nanostructures. Hence, the theoretical predictions of this work are supported by prior studies [3], strengthening the conclusion that larger pyrene clusters offer improved sensing performance for highly toxic gases.

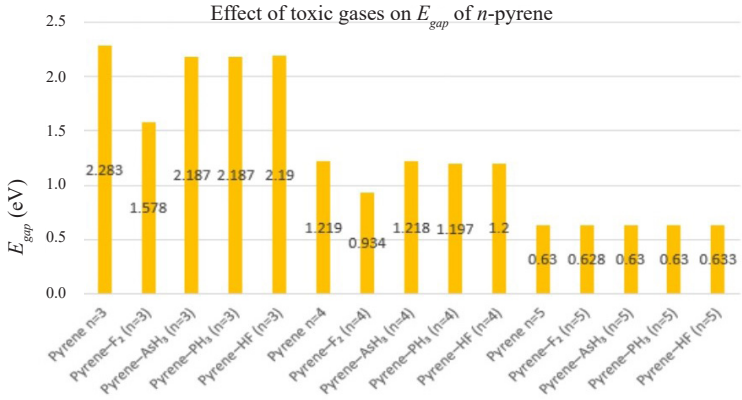

Fig. 5. The change of energy gap (E_{gap}) of n-pyrene upon adsorption of toxic gases of different nature

Table 3

Calculated characteristics of the electronic properties of pristine pyrene (n = 3 – 5) and the pyrene with high toxic gases adsorbed

System	Parameter value, eV			σ, 1/eV
	IP	EA	η	
3-pyrene (3P)				
Pristine 3P	4.596	2.313	1.142	0.438
3P–F_2	4.891	3.312	0.789	0.634
3P–AsH_3	4.569	2.381	1.094	0.457
3P–PH_3	4.593	2.406		
3P–HF	4.778	2.588	1.095	0.456
4-pyrene (4P)				
Pristine 4P	4.171	2.952	0.610	0.820
4P–F_2	4.347	3.413	0.467	1.071
4P–AsH_3	4.169	2.951	0.609	0.821
4P–PH_3	4.134	2.937	0.598	0.836
4P–HF	4.256	3.055	0.600	0.833
5-pyrene (5P)				
Pristine 5P	3.919	3.289	0.315	1.588
5P–F_2	4.107	3.480	0.314	1.593
5P–AsH_3	3.925	3.295	0.315	1.587
5P–PH_3	3.905	3.274		
5P–HF	3.977	3.345	0.316	1.581

Notations: IP is the ionization potential, EA is the electron affinity; η, σ are chemical hardness and softness, relatively.

Global reactivity descriptors. The electronic properties ionization potential (IP), electron affinity (EA), electronegativity and electrophilicity classified as global merits [32]. The ionization potential is the lowest energy required to remove an electron from an atom. It can be measured for each electron of the atom (according to Koopmans theorem).

Table 3 presents the ionization potential (IP), electron affinity (EA), chemical hardness (η), and softness (σ) of pyrene nanostructures of different sizes (n = 3 – 5) functionalized with toxic gases (F_2, AsH_3, PH_3, and HF). These descriptors provide further insight into the electronic stability and reactivity of the adsorption complexes. The pristine pyrene nanostructures exhibit relatively high IP values:

4.59 eV for n = 3; 4.17 eV for n = 4;
and 3.92 eV for n = 5,

which decrease slightly with the system sizes.

This result reflects a decrease in the energy required to remove an electron as the π-system becomes more delocalized. Upon adsorption, IP values vary depending on the gas nature; such as F_2 and HF generally increase IP slightly, suggesting stabilization of the electronic structure, while AsH_3 and PH_3 tend to lower IP values, making the system more prone to electron donation, which is favorable for sensory applications [33].

This result reflects a decrease in the energy required to remove an electron because the π-system becomes more delocalized. Upon

adsorption, IP values vary depending on the gas nature; such as F_2 and HF generally increase IP slightly, suggesting stabilization of the electronic structure, while AsH_3 and PH_3 tend to lower IP values, making the system more sensitive to electron donation, which is favorable for sensory applications [33]. The electron affinity also increases significantly upon adsorption of all gases, particularly for F_2 and HF (up to 3.34 eV). This points out an enhanced tendency of the system to accept electrons, consistent with a charge transfer from the adsorbates to the pyrene structure. The elevated EA values highlight the potential for improved sensitivity in electron-mediated detection mechanisms.

Hardness η decreases markedly upon adsorption. For instance, pristine pyrene has $\eta \approx 1.14$ eV for $n = 3$, while adsorption of AsH_3 or F_2 reduces it below 0.6 eV in some cases. A lower hardness value corresponds to increased chemical reactivity and reduced electronic stability. Conversely, the softness value increases significantly upon adsorption, especially for larger systems (for instance, $\sigma > 1.5$ $(eV)^{-1}$ at $n = 5$). This shift toward higher softness indicates enhanced polarizability and stronger electronic responsiveness, being desirable characteristics for sensing materials.

Table 4

Electronegativity, electrophilicity, polarizability, and dipole moment for pristine *n*-pyrene ($n = 3 - 5$) and those with high toxic gases

System	Parameter value			
	χ, eV	ω, eV	α, a.u.	μ, D
3-pyrene (3P)				
Pristine 3P	–3.454	5.227	399.144	$1.1 \cdot 10^{-6}$
3P–F_2	–4.101	10.659	431.956	4.984
3P–AsH_3	–3.475	5.521	429.817	0.746
3P–PH_3	–3.500	5.600	421.206	1.210
3P–HF	–3.683	6.192	402.349	3.085
4-pyrene (4P)				
Pristine 4P	–3.561	10.407	819.759	$6.2 \cdot 10^{-5}$
4P–F_2	–3.880	16.116	845.641	4.370
4P–AsH_3	–3.560	10.402	839.140	0.475
4P–PH_3	–3.535	10.444	836.159	1.142
4P–HF	–3.656	11.130	821.186	2.220
5-pyrene (5P)				
Pristine 5P	–3.604	20.621	1468.848	$8.7 \cdot 10^{-5}$
5P–F_2	–3.793	22.925	1485.465	4.933
5P–AsH_3	–3.610	20.682	1485.778	0.251
5P–PH_3	–3.590	20.446	1483.693	1.137
5P–HF	–3.661	21.186	1470.188	2.072

Notations: χ is the electronegativity, ω is the electrophilicity, α is the polarizability, μ is the dipole moment.

Based on the results presented in Table 4, the highest electronegativity values are observed in the following systems:

System	χ, eV
3-pyrene-F_2	− 4.10
4-pyrene-F_2	−3.88
5-pyrene-F_2	−3.793.

The adsorption or interaction of fluorine gas leads to an increase in the electronegativity of the compound, which enhances its ability to attract electrons which is an important factor in chemical reactivity.

As for polarizability, we observe the following high values:

System	α, a.u.
5-pyrene-HF	1470.18
5-pyrene-PH_3	1483.69
5-pyrene-AsH_3	1485.77

Polarizability increases at the $n = 5$ graphene-diamond surface, and its interaction with gases makes the surface electronically polarized. This fact is beneficial for applications in sensitive devices and conductivity. Regarding electrophilicity, it increases significantly at $n = 5$, with values ranging between ~20.446 and 22.92 eV, indicating higher chemical reactivity and a stronger tendency to accept electrons. As for the dipole moment μ, it reflects the asymmetry in charge distribution. High values of the dipole moments are seen in systems such as 3-pyrene-F_2 (μ = 4.984 D), indicating a strong charge asymmetry and an ability to interact with external electric fields. On the other hand, the lowest values are observed in the pristine pyrene systems with $n = 3$, 4, and 5, reflecting a highly symmetric and electronically stable configuration.

Table 5

Total and adsorption energies for pristine pyrene ($n = 3 - 5$) and pyrene with toxic gases adsorbed

System	Energy parameter value		
	E_{tot}, a.u. (Hartree)	E_{ads}	
		eV	kJ/mol
3-pyrene (3P)			
Pristine 3P	–1151.49	–	
3P–F_2	–1350.98	–0.4009	–38.6867
3P–AsH_3	–3386.84	–2.0925	–201.900
3P–PH_3	–1494.59	–1.3019	–125.617
3P–HF	–1251.9	–0.1499	–14.4665
4-pyrene (4P)			
Pristine 4P	–1839.76	–	
4P–F_2	–2039.25	–0.2975	–28.7098
4P–AsH_3	–4075.10	–1.8411	–177.647
4P–PH_3	–2182.87	–1.2497	–120.584
4P–HF	–1940.17	–0.1358	–13.1065
5-pyrene (5P)			
Pristine 5P	–2680.47	–	
5P–F_2	–2879.96	–0.3469	–33.4725
5P–AsH_3	–4915.81	–1.9253	–185.773
5P–PH_3	–3023.57	–1.2603	–121.608
5P–HF	–2780.88	–0.1209	–11.6651

The total energy and adsorption energy

The total energy is calculated as the sum of the kinetic energy of the electrons, the nucleus-electrons interaction energy, and the electron-electron repulsion energy, while represents the exchange-correlation term [34, 35].

The data in Table 5 demonstrates the calculated total and adsorption energies in both electronvolts (eV) and kilojoules per mole (kJ/mol) for pyrene nanostructures of different sizes ($n = 3 - 5$) upon functionalization with F_2, AsH_3, PH_3, and HF. The total energy becomes progressively more negative as the pyrene size increases

(−1151.49, −1839.76, and −2680.47 a.u. for n =3, 4, and 5, respectively),

consistent with the stabilization gained from an extended π-conjugated system.

This trend confirms that larger pyrene nanostructures provide more thermodynamically favorable adsorption surfaces. The adsorption energies reveal a clear distinction between strong and weak interactions. In this way, the chemisorption occurs for PH_3 and AsH_3, particularly AsH_3, which exhibits very high adsorption energies (up to 5.35 eV, or 516 kJ/mol at $n = 5$). Such large values indicate the significant orbital hybridization and charge redistribution

between the toxic gas and the pyrene surface. At the same time, the weak physisorption is observed for F_2 and HF, with adsorption energies ranging from −0.12 to −0.40 eV (from −11.6 to −38.7 kJ/mol). These values are comparable to Van der Waals interactions, suggesting minimal charge transfer. For instance, the AsH_3 consistently shows the strongest binding over all pyrene sizes, reflecting its high chemical reactivity and strong donor-acceptor interactions with the π-framework, whereas the PH_3 adsorption is also substantial:

from −1.26 to −1.30 eV (or −121 to −126 kJ/mol),

although weaker than that of AsH_3.

On the other hand, both F_2 and HF remain weakly bound, highlighting their role as stabilizing modifiers rather than strong dopants.

Summing up, from an application perspective, the strong chemisorption of AsH_3 and PH_3 makes pyrene derivatives highly promising for toxic gas detection and capture technologies, as the adsorption is both energetically favorable and electronically disruptive. Conversely, the weaker physisorption of F_2 and HF suggests potential utility in situations where reversible adsorption is desirable, such as catalytic cycles or reusable sensors.

Conclusions

The findings of this study have shown that molecular adsorption of toxic gases induces significant modifications in the electronic structure of the host systems, governed by both the chemical nature of the adsorbate and the dimensional scale of the molecular substrate. Among the investigated species, F_2 and HF emerge as the most effective candidates for electronic detection, exhibiting marked alterations in conductivity upon interaction. This behavior is particularly enhanced in extended π-conjugated frameworks such as $C_{70}H_{22}$, highlighting the potential of large-scale organic systems in the development of nanoscale gas sensors with high sensitivity and selectivity toward hazardous gaseous environments. As the pyrene size increases, the descriptors shift toward greater reactivity (lower IP and η values, higher EA and σ values). This suggests that larger pyrene nanostructures are more chemically active and more sensitive to adsorption-induced perturbations, making them better candidates for real-world sensing applications.

Acknowledgments

The authors express their graduate to the leadership of the Department of Physics and College of Science (University of Thi-Qar) for assistance in fulfilling a part of the requirements for obtaining a Master's degree.

REFERENCES

1. **Kumar Y., Sahoo S., Chakraborty A. K.,** Mechanical properties of graphene, defective graphene, multilayer graphene and SiC-graphene composites: A molecular dynamics study, Phys. B: Cond. Matter, 620 (1 Nov) (2021) 413250.

2. **Elmghabar Z., Elidrysy A., Harir S., Drissi L.,** Magnetic properties and magnetocaloric effect of diamond-shaped graphene bilayer quantum dots doped with magnetic impurities: A Monte Carlo study, J. Magn. Magn. Mater. 608 (15 Oct) (2024) 172443.

3. **Huang H.-J., Seenithurai S., Chai J.-D.,** TAO-DFT study on the electronic properties of diamond-shaped graphene nanoflakes, Nanomaterials. 10 (6) (2020) 1236.

4. **Omeer T. A., Mohammed M. H.,** Tuning the band gap in graphene nanoflakes via various impurities, Nano-Struct. Nano-Objs. 35 (July) (2023) 101009.

5. **Batool D. B., Fallah H. H., Alwan A. S.,** Geometrical optimization and some physical properties for sodium on copper clusters, IOSR J. Appl. Phys. 7 (3-Ver. II) (2015) 30−37.

6. **Aldulaijan S., Ajeebi A. M., Jedidi A., et al.,** Surface modification of graphene with functionalized carbenes and their applications in the sensing of toxic gases: a DFT study, RSC Adv. 13 (28) (2023) 19607−19616.

7. **Jabbar M. L., Al-Shejairy K. J.,** A new fractal geometry doping for graphene nanoribbon and the optimization of crystal: A density functional theory (DFT) study, Per. Tchê Quím. 17 (35) (2020) 1148−1158.

8. **Jabbar M. L., Kadhim K. J.,** Linear & nonlinear optical properties of undoped & doped graphene nanoribbon via TD-DFT study, AIP Conf. Proc. 2292 (1) (2020) 030011.

9. **Benítez-Martínez S., Valcárcel M.,** Graphene quantum dots in analytical science, Trends Anal. Chem. 72 (Oct) (2015) 93–113.

10. **Bao Q., Yang Z., Lu Z., He X.,** Effects of graphene thickness and length distribution on the mechanical properties of graphene networks: A coarse-grained molecular dynamics simulation, Appl. Surf. Sci. 570 (30 Dec) (2021) 151023.

11. **Leenaerts O., Partoens B., Peeters F. M.,** Adsorption of small molecules on graphene, Microelectron. J. 40 (4–5) (2009) 860–862.

12. **Guerra T., Araujo L., Azevedo S.,** Magnetic and electronic properties of diamond-shaped graphene-boron nitride nanoribbons and nanoflakes, J. Phys. Chem. Solids. 135 (Dec) (2019) 109085.

13. **Yang J., Zhang Y., Kim D. Y.,** Electrochemical sensing performance of nanodiamond-derived carbon nano-onions: Comparison with multiwalled carbon nanotubes, graphite nanoflakes, and glassy carbon, Carbon. 98 (March) (2016) 74–82.

14. **Lahiani M. H., Chen J., Irin F., et al.,** Interaction of carbon nanohorns with plants: Uptake and biological effects, Carbon. 81 (Jan) (2015) 607–619.

15. **Zhang X., Rajaraman B. R., Liu H., Ramakrishna S.,** Graphene's potential in materials science and engineering, RSC Adv. 4 (55) (2014) 28987–29011.

16. **Deng Q., Chai J.-D.,** Electronic properties of triangle-shaped graphene nanoflakes from TAO-DFT, ACS Omega. 4 (10) (2019) 14202–14210.

17. **Thu P. T., Mai N. T., Lien P. T., Tung N. T.,** Magnetism in diamond graphene nanoflakes, Vietnam J. Sci. Technol. 61 (1) (2023) 64–71.

18. **Jabbar M. L., Kadhim K. J.,** Electronic properties of doped graphene nanoribbon and the electron distribution contours: A DFT study, Russ. J. Phys. Chem. B. 15 (1) (2021) 46–52.

19. **Sarmada A., Pupon S.,** The external electric field effect to hydrogen storage on BN co-doped graphene surface decorated by metal atoms: A DFT study, J. Phys. Sci. Eng. 4 (2) (2020) 74–83.

20. **Xiang C., Li A., Yang S., Lan Z.,** Enhanced hydrogen storage performance of graphene nanoflakes doped with Cr atoms: a DFT study, RSC Adv. 9 (44) (2019) 25690–25696.

21. **Kishnani V., Yadav A., Mondal K., Gupta A.,** Palladium-functionalized graphene for hydrogen sensing performance: theoretical studies, Energies. 14 (18) (2021) 5738.

22. **Cruz-Martínez H., García-Hilerio B., Montejo-Alvaro F., et al.,** Density functional theory-based approaches to improving hydrogen storage in graphene-based materials, Molecules. 29 (2) (2024) 436.

23. **Cruz-Martínez H., Rojas-Chávez H., Montejo-Alvaro F., et al.,** Recent developments in graphene-based toxic gas sensors: a theoretical overview, Sensors. 21 (6) (2021) 1992.

24. **Alwan A. S., Talib S. H.,** Quantum computational study of the electronic properties of the interactions between 3THF and some metallic linear molecules using DFT, J. Educ. Pure Sci. 11 (2) (2021) 53–67.

25. **Toriyama M. A., Ganose A. M., Dylla M., Anand S.,** How to analyze a density of states, Mater. Today Electron. 1 (May) (2022) 100002.

26. **Aqeel S., Shwya A.,** Molecular geometry and electronic characteristics of zirconium and (zirconium-Ge, Si, Sn) utilizing density functional theory (DFT) codes at 3-21G basis set, NeuroQuantology. 20 (8) (2022) 2767–2778.

27. **Ahmed A. B.,** Studying the electronic characteristics and physisorption of OTS on the pure silver surfaces (Ag_{10}), (Ag_{15}) and (Ag_{18}), Univ. Thi-Qar J. Sci. 10 (2) (2023) 151–159.

28. **Alwan A. Sh., Ajeel S. Kh., Jabbar M. L.,** Theoretical study for Coronene and Coronene-Al, B, C, Ga, In and Coronene-O interactions by using Density Functional Theory, Univ. Thi-Qar J. 14 (4) (2019) 80–94.

29. **Salih F. T., Alwan A. Sh.,** Charge transfer and physisorption mechanism between tosylate, pyrimidine and the surfaces of nanocopper (Cu) and (Cu) utilizing algorithms of (DFT), J. Educ. Pure Sci. 13 (4) (2023) 74–96.

30. **Talib S. H., Alwan A. Sh.,** Geometrical optimization and some electronical properties for pyrrole-metal interactions using DFT, B3LYP basis sets, J. Optoelectron. Laser. 41 (7) (2022) 1300–1312.

31. **Sengul O., Völkle J., Valli A., Stadler R.,** Enhancing the sensitivity and selectivity of pyrene-based sensors for detection of small gaseous molecules via destructive quantum interference, Phys. Rev. B. 105 (16) (2022) 165428.

32. **Muhsen H. O., Kadhim B. B., Almayyali A. O. M.,** Electronic properties of InPNT drug carrier, J. Chem. Pharm. Sci. 10 (3) (2017) 1414–1418.

33. **Nasri A., Petrissans M., Fierro V., Celzard A.,** Gas sensing based on organic composite materials: Review of sensor types, progresses and challenges, Mater. Sci. Semicond. Proc. 128 (15 June) (2021) 105744.

34. **Haken H., Wolf H. C.,** Molecular physics and elements of quantum chemistry: Introduction to experiments and theory. 2nd ed. (Book Ser. "Advanced Texts in Physics (ADTP)"), Springer Science & Business Media, Berlin, Heidelberg, 2004.

35. **Thierfelder C., Witte M., Blankenburg S., et al.,** Methane adsorption on graphene from first principles including dispersion interaction, Surf. Sci. 605 (7–8) (2011) 746–749.

СПИСОК ЛИТЕРАТУРЫ

1. **Kumar Y., Sahoo S., Chakraborty A. K.** Mechanical properties of graphene, defective graphene, multilayer graphene and SiC-graphene composites: A molecular dynamics study // Physica B: Condensed Matter. 2021. Vol. 620. 1 November. P. 413250.

2. **Elmghabar Z., Elidrysy A., Harir S., Drissi L.** Magnetic properties and magnetocaloric effect of diamond-shaped graphene bilayer quantum dots doped with magnetic impurities: A Monte Carlo study // Journal of Magnetism and Magnetic Materials. 2024. Vol. 608. 15 October. P. 172443.

3. **Huang H.-J., Seenithurai S., Chai J.-D.** TAO-DFT study on the electronic properties of diamond-shaped graphene nanoflakes // Nanomaterials. 2020. Vol. 10. No. 6. P. 1236.

4. **Omeer T. A., Mohammed M. H.** Tuning the band gap in graphene nanoflakes via various impurities // Nano-Structures & Nano-Objects. 2023. Vol. 35. July. P. 101009.

5. **Batool D. B., Fallah H. H., Alwan A. S.** Geometrical optimization and some physical properties for sodium on copper clusters // IOSR Journal of Applied Physics. 2015. Vol. 7. No. 3 (Version II). Pp. 30–37.

6. **Aldulaijan S., Ajeebi A. M., Jedidi A., Messaoudi S., Raouafi N., Dhouib A.** Surface modification of graphene with functionalized carbenes and their applications in the sensing of toxic gases: a DFT study // RSC (The Royal Society of Chemistry) Advances. 2023. Vol. 13. No. 28. Pp. 19607–19616.

7. **Jabbar M. L., Al-Shejairy K. J.** A new fractal geometry doping for graphene nanofibers and crystal optimization: A study of functional density theory (FDD) // Periydico Tchê Química. 2020. Vol. 17. No. 35. Pp. 1148–1158.

8. **Jabbar M. L., Kadhim K. J.** Linear & nonlinear optical properties of undoped & doped graphene nanoribbon via TD-DFT study // AIP Conference Proceedings. 2020. Vol. 2292. No. 1. P. 030011.

9. **Benítez-Martínez S., Valcárcel M.** Graphene quantum dots in analytical science // Trends in Analytical Chemistry. 2015. Vol. 72. October. Pp. 193–113.

10. **Bao Q., Yang Z., Lu Z., He X.** Effects of graphene thickness and length distribution on the mechanical properties of graphene networks: A coarse-grained molecular dynamics simulation // Applied Surface Science. 2021. Vol. 570. 30 December. P. 151023.

11. **Leenaerts O., Partoens B., Peeters F. M.** Adsorption of small molecules on graphene // Microelectronics Journal. 2009. Vol. 40. No. 4–5. Pp. 860–862.

12. **Guerra T., Araujo L., Azevedo S.** Magnetic and electronic properties of diamond-shaped graphene-boron nitride nanoribbons and nanoflakes // Journal of Physics and Chemistry of Solids. 2019. Vol. 135. December. P. 109085.

13. **Yang J., Zhang Y., Kim D. Y.** Electrochemical sensing performance of nanodiamond-derived carbon nano-onions: Comparison with multiwalled carbon nanotubes, graphite nanoflakes, and glassy carbon // Carbon. 2016. Vol. 98. March. Pp. 74–82.

14. **Lahiani M. H., Chen J., Irin F., Puretzky A. A., Green M. J., Khodakovskaya M. V.** Interaction of carbon nanohorns with plants: uptake and biological effects // Carbon. 2015. Vol. 81. January. Pp. 607–619.

15. **Zhang X., Rajaraman B. R., Liu H., Ramakrishna S.** Graphene's potential in materials science and engineering // RSC Advances. 2014. Vol. 4. No. 55. Pp. 28987–29011.

16. **Deng Q., Chai J.-D.** Electronic properties of triangle-shaped graphene nanoflakes from TAO-DFT // ACS Omega. 2019. Vol. 4. No. 10. Pp. 14202–14210.

17. **Thu P. T., Mai N. T., Lien P. T., Tung N. T.** Magnetism in diamond graphene nanoflakes // Vietnam Journal of Science and Technology. 2023. Vol. 61. No. 1. Pp. 64–71.

18. **Jabbar M. L., Kadhim K. J.** Electronic properties of doped graphene nanoribbon and the electron distribution contours: A DFT study// Russian Journal of Physical Chemistry B. 2021. Vol. 15. No. 1. Pp. 46–52.

19. **Sarmada A., Pupon S.** The external electric field effect to hydrogen storage on BN co-doped graphene surface decorated by metal atoms: A DFT study // Journal of Physical Science and Engineering. 2020. Vol. 4. No. 2. Pp. 74–83.

20. **Xiang C., Li A., Yang S., Lan Z.** Enhanced hydrogen storage performance of graphene nanoflakes doped with Cr atoms: A DFT study// RSC Advances. 2019. Vol. 9. No. 44. Pp. 25690–25696.

21. **Kishnani V., Yadav A., Mondal K., Gupta A.** Palladium-functionalized graphene for hydrogen sensing performance: theoretical studies // Energies. 2021. Vol. 14. No. 18. P. 5738.

22. **Cruz-Martínez H., García-Hilerio B., Montejo-Alvaro F., Gazga-Villalobos A., Rojas-Chávez H., Sánchez-Rodríguez E. P.** Density functional theory-based approaches to improving hydrogen storage in graphene-based materials // Molecules. 2024. Vol. 29. No. 2. P. 436.

23. **Cruz-Martínez H., Rojas-Chávez H., Montejo-Alvaro F., Peca-Castaceda Y. A., Matadamas-Ortiz P. T., Medina D. I.** Recent developments in graphene-based toxic gas sensors: a theoretical overview // Sensors. 2021. Vol. 21. No. 6. P. 1992.

24. **Alwan A. S., Talib S. H.** Quantum computational study of the electronic properties of the interactions between 3THF and some metallic linear molecules using DFT // Journal of Education for Pure Science. 2021. Vol. 11. No. 2. Pp. 53–67.

25. **Toriyama M. A., Ganose A. M., Dylla M., Anand S.** How to analyze a density of states // Materials Today Electronics. 2022. Vol. 1. May. P. 100002.

26. **Aqeel S., Shwya A.** Molecular geometry and electronic characteristics of zirconium and (zirconium-Ge, Si, Sn) utilizing density functional theory (DFT) codes at 3-21G basis set // NeuroQuantology. 2022. Vol. 20. No. 8. Pp. 2767–2778.

27. **Ahmed A. B.** Studying the electronic characteristics and physisorption of OTS on the pure silver surfaces (Ag_{10}), (Ag_{15}) and (Ag_{18}) // University of Thi-Qar Journal of Science. 2023. Vol. 10. No. 2. Pp. 151–159.

28. **Alwan A. Sh., Ajeel S. Kh., Jabbar M. L.** Theoretical study for Coronene and Coronene-Al, B, C, Ga, In and Coronene-O interactions by using Density Functional Theory // University of Thi-Qar Journal. 2019. Vol. 14. No. 4. Pp. 80–94.

29. **Salih F. T., Alwan A. Sh.** Charge transfer and physisorption mechanism between tosylate, pyrimidine and the surfaces of nanocopper (Cu) and (Cu) utilizing algorithms of (DFT) // Journal of Education for Pure Science. 2023. Vol. 13. No. 4. Pp. 74–96.

30. **Talib S. H., Alwan A. Sh.** Geometrical optimization and some electronical properties for pyrrole-metal interactions using DFT, B3LYP basis sets // Journal of Optoelectronics Laser. 2022. Vol. 41. No. 7. Pp. 1300–1312.

31. **Sengul O., Völkle J., Valli A., Stadler R.** Enhancing the sensitivity and selectivity of pyrene-based sensors for detection of small gaseous molecules via destructive quantum interference // Physical Review B. 2022. Vol. 105. No. 16. P. 165428.

32. **Muhsen H. O., Kadhim B. B., Almayyali A. O. M.** Electronic properties of InPNT drug carrier // Journal of Chemical and Pharmaceutical Sciences. 2017. Vol. 10. No. 3. Pp. 1414–1418.

33. **Nasri A., Petrissans M., Fierro V., Celzard A.** Gas sensing based on organic composite materials: Review of sensor types, progresses and challenges // Materials Science in Semiconductor Processing. 2021. Vol. 128. 15 June. P. 105744.

34. **Haken H., Wolf H. C.** Molecular physics and elements of quantum chemistry: Introduction to experiments and theory. 2nd edition (Book Series “Advanced Texts in Physics (ADTP)”). Berlin, Heidelberg: Springer Science & Business Media, 2004. 596 p.

35. **Thierfelder C., Witte M., Blankenburg S., Rauls E., Schmidt W.** Methane adsorption on graphene from first principles including dispersion interaction // Surface Science. 2011. Vol. 605. No. 7–8. Pp. 746–749.

THE AUTHORS

KHALAF Rihab H.
University of Thi-Qar, Department of Physics, College of Science
University of Thi-Qar 362C+65R, An Nasiriyah, Thi-Qar Governorate, 64001, Republic of Iraq.
rihab.khalaf@utq.edu.iq

JABBAR Mohammed L.
University of Thi-Qar, Department of Physics, College of Science
University of Thi-Qar, 362C+65R, An Nasiriyah, Thi-Qar Governorate, 64001, Republic of Iraq.
mohammed25382@gmail.com
ORCID: 0009-0003-4737-7008

СВЕДЕНИЯ ОБ АВТОРАХ

ХАЛАФ Рихаб Х. – *магистр наук, сотрудник кафедры физики Научного колледжа Университета Ди-Кар, г. Эн-Насирия, Республика Ирак.*
362C+65R, Republic of Iraq, Thi-Qar Governorate, An Nasiriyah, University of Thi-Qar.
rihab.khalaf@utq.edu.iq

ДЖАББАР Мохаммед Л. – *PhD, доцент кафедры физики Научного колледжа Университета Ди-Кар, г. Эн-Насирия, Республика Ирак.*
362C+65R, Republic of Iraq, Thi-Qar Governorate, Nasiriyah, University of Thi-Qar.
mohammed25382@gmail.com
ORCID: 0009-0003-4737-7008

Received 02.09.2025. Approved after reviewing 05.11.2025. Accepted 07.11.2025.
Статья поступила в редакцию 02.09.2025. Одобрена после рецензирования 05.11.2025. Принята 07.11.2025.